Journal of Alloys and Compounds 504S (2010) S311–S314

Contents lists available at ScienceDirect

Journal of Alloys and Compounds

journal homepage: www.elsevier.com/locate/jallcom

Synthesis and characterization of nanocrystalline Mg_2Ni prepared by mechanical alloying: Effects of substitution of Mn for Ni

L.W. Huang[a,*], O. Elkedim[a], V. Moutarlier[b]

[a] FEMTO-ST, MN2S, Université de Technologie de Belfort-Montbéliard, Site de Sévenans, 90010 Belfort cedex, France
[b] Institut UTINAM, UMR 6213, 16 Route de Gray, 25000 Besançon, France

ARTICLE INFO

Article history:
Received 3 July 2009
Received in revised form 4 January 2010
Accepted 10 February 2010
Available online 18 February 2010

Keywords:
Mg_2Ni alloy
Mn
Mechanical alloying
Nanocrystalline
Elemental substitution

ABSTRACT

The $Mg_2Ni_{(1-x)}Mn_x$ ($x = 0, 0.125, 0.25, 0.375$) hydrogen storage alloys have been synthesized by mechanical alloying (MA). The effects of substitution of Mn for Ni on the phase composition and microstructures of Mg_2Ni-type alloys have been investigated by X-ray diffraction (XRD) and scanning electron microscopy (SEM). XRD results of milled samples indicate that substitution of Mn for Ni could inhibit the formation of $MgNi_2$ phase and the solid solubility of Mn in Mg_2Ni phase is low. The calculation of average crystallite size and microstrain of $Mg_2Ni_{(1-x)}Mn_x$ alloys milled for 8 h shows that with the increase of substitution amount of Mn for Ni from $x = 0$ to $x = 0.375$, the average crystallite size decreases first from 12.5 nm to 9.6 nm and then increases from 9.6 nm to 11.8 nm with the minimum 9.6 nm obtained at $x = 0.25$, while the microstrain monotonously decreases from 1.39% to 0.82%. SEM has revealed that the sizes of subparticles that constitute the powder particles in the composition $Mg_2Ni_{0.75}Mn_{0.25}$ are much smaller than those in other compositions.

1. Introduction

Many intermetallic compounds are attractive candidates for hydrogen storage due to their capability of reversibly absorbing large amounts of hydrogen. If AB_n ($n = 0.5, 1, 2, 5$) is used to denote the binary intermetallic compounds for hydrogen storage, element A is usually a rare earth (e.g. La), an alkaline earth metal (e.g. Mg) or former transition metal (e.g. Ti, Zr) and tends to form a highly stable hydride at room temperature. Whereas element B is often a latter transition metal (e.g. Fe, Ni, Cu) and does not form stable hydrides at room temperature [1–3]. The combination of different elements in AB_n can be used to design and tailor the properties, such as Mg_2Ni [4], TiFe [5], ZrV_2 [6] and $LaNi_5$ [7]. Mg_2Ni intermetallic compound is one of the most promising alloys in the AB_n family, since besides its lightweight and low cost, its theoretical gravimetric storage hydrogen capacity, assuming the formation of Mg_2NiH_4, is 3.6 mass% (equivalent to 999 mAh/g for the discharge capacity, which is approximately 2.7 times that of $LaNi_5$) and it can absorb and desorb hydrogen at more moderate temperatures and pressures than other alloys. However, the poor hydriding/dehydriding kinetics and high thermodynamical stability of Mg_2NiH_4 (requiring 280 °C for 1 bar hydrogen [8]) become the obstacle for the practical use for hydrogen storage.

There are many methods to improve the hydrogen storage properties or electrochemical hydrogen storage properties of Mg_2Ni intermetallic compound: (a) adding suitable catalysts [4,9]; (b) increasing specific surface area [10]; (c) substituting partial elements [11–13] and (d) using new synthesis methods to decrease the crystallite size to nanoscale (such as mechanical alloying [4], polyol reduction method [14]). Mechanical alloying (MA) is a solid-state powder processing technique involving repeated welding, fracturing, and rewelding of powder particles in a high-energy ball mill [15]. This method is considered to be more appropriate for synthesizing Mg_2Ni intermetallic compound than conventional metallurgical methods, such as melting, because of the low miscibility of Mg with most transition metals, the high vapor pressure of Mg and the difference between Mg and Ni melting points. Nanocrystalline Mg_2Ni produced by MA showed substantially enhanced absorption and desorption kinetics, even at relatively low temperatures [16].

Yang et al. [17] found that replacement of Ni in Mg_2Ni by Mn lowered the decomposition plateau pressure. Kohno and Kanda [18] reported that as a result of substitution of Mg with Mn, absorption of hydrogen occurred at lower temperature. Gasiorowski et al. [12] found that the partial substitution of Mg by Mn in Mg_2Ni alloy leaded to an increase in discharge capacities at room temperature. It can be seen that different authors used different substitution methods. Some used Mn to substitute Ni, while others used Mn to substitute Mg in Mg_2Ni. Tsushio and Akiba [19] proposed that for designing a quaternary alloy system of Mg_2Ni by substitution

* Corresponding author.
E-mail address: liwu.huang@utbm.fr (L.W. Huang).

0925-8388/$ – see front matter © 2010 Elsevier B.V. All rights reserved.
doi:10.1016/j.jallcom.2010.02.059

Table 1
Phase composition of $Mg_2Ni_{(1-x)}Mn_x$ (x = 0, 0.125, 0.25, 0.375) alloys for different milling times.

Sample	Phase composition			
	4 h	8 h	16 h	24 h
Mg_2Ni	Mg, Ni, traces of Mg_2Ni	Mg_2Ni, $MgNi_2$	Mg_2Ni, $MgNi_2$	Mg_2Ni, $MgNi_2$
$Mg_2Ni_{0.875}Mn_{0.125}$	Mg, Ni, Mn	Mg_2Ni, Mn, traces of $MgNi_2$	Mg_2Ni, Mn, traces of $MgNi_2$	Mg_2Ni, Mn, traces of $MgNi_2$
$Mg_2Ni_{0.75}Mn_{0.25}$	Mg, Ni, Mn	Mg_2Ni, Mn	Mg_2Ni, Mn	Mg_2Ni, Mn
$Mg_2Ni_{0.625}Mn_{0.375}$	Mg, Ni, Mn	Mg_2Ni, Mn	Mg_2Ni, Mn	Mg_2Ni, Mn

method, the substitution for Ni had to be considered first and then for Mg. However, the literatures that reported using the different substitution ratios of Mn for Ni in Mg_2Ni alloy to study the effects are few.

The purpose of this work is to synthesize the $Mg_2Ni_{(1-x)}Mn_x$ (x = 0, 0.125, 0.25, 0.375) alloys by MA and to investigate the effects of substitution of Mn for Ni on the phase composition and microstructures of Mg_2Ni-type alloys systematically for providing a guide for improving the hydrogen storage properties of Mg_2Ni intermetallic compound.

2. Experimental procedure

Starting elemental powders of Mg (purity 99.8%, particle size ≤50 μm, from GoodFellow), Ni (purity 99.5%, particle size ≤250 μm, from GoodFellow) and Mn (particle size −325 mesh, purity 99.3%, from Alfa) were mixed and poured into the stainless steel vials (volume 50 ml) together with two stainless steel balls (diameter 20 mm) in the glove box filled with argon according to the designed composition $Mg_2Ni_{(1-x)}Mn_x$ (x = 0, 0.125, 0.25, 0.375). The MA was carried out with 20:1 ball to powder weight ratio under argon atmosphere at room temperature using a planetary high-energy ball mill (Retsch PM 400) at a speed of 400 rpm. The milling was interrupted for 30 min/h to dissipate the heat and to reduce the excessive rise of temperature.

The structures of the MA alloys with different compositions milled for different periods of time were analyzed by the Bruker D8 Advance X-ray diffractometer with Cu Kα radiation (λ = 0.15418 nm) filtered by nickel. The crystallite size and microstrain were calculated from the approximation (Eq. (1)) that combines the Wilson formula and Scherrer formula following Williamson–Hall style plot [20].

$$\beta = 2\varepsilon \tan\theta + \frac{0.9\lambda}{d\cos\theta} \quad (1)$$

where β is the full-width at half maximum intensity of a Bragg reflection excluding instrumental broadening, θ the Bragg angle, λ the wavelength of the X-ray radiation, ε the effective lattice microstrain and d the average crystallite size.

The morphologies of the powdered samples were observed using the JEOL JSM-5800LV Scanning Electron Microscope.

3. Results and discussion

Fig. 1 shows the evolution of X-ray diffraction patterns of $Mg_2Ni_{(1-x)}Mn_x$ (x = 0, 0.125, 0.25, 0.375) alloys mechanically alloyed for 8 h. It can be seen that all MA alloys exhibit new diffraction peaks, which are identified as Mg_2Ni or $MgNi_2$ phase. The Mg_2Ni phase exists in all composition, whereas $MgNi_2$ phase gradually decreases with the increase of x (the content of Mn) and disappears as x achieves 0.25 and 0.375. Phase composition of $Mg_2Ni_{(1-x)}Mn_x$ (x = 0, 0.125, 0.25, 0.375) alloys for different milling times is displayed in Table 1. This phenomenon indicates that substitution of Mn for Ni could inhibit the formation of $MgNi_2$ phase, which is possibly ascribed to the change of atom ratios between Mg and Ni. During mechanical alloying, since Mg is very soft and easier to adhere to the balls and walls of vials, the real content of Ni is above and near to 33 at% for x = 0 and x = 0.125 (smaller amount of substitution), respectively, which is corresponding to the $Mg_2Ni + MgNi_2$ region in the Mg–Ni system. Therefore, Mg_2Ni and small amount of $MgNi_2$ phases coexist for x = 0 and 0.125. After large amount of substitution of Mn for Ni, Ni content is below 33 at%, which belongs to the $Mg_2Ni + Mg$ region. As a result, $MgNi_2$ phase disappears when x = 0.25 and 0.375. In contrast to Mg_2Ni, the $MgNi_2$ phase does not interact with hydrogen [21], so the substitution of Mn for Ni is favorable for synthesizing the single Mg_2Ni phase and improve the hydrogen storage capacity by promoting the reaction of Mg and Ni to form Mg_2Ni phase. It is also noted that the peaks of Mn phase still exist in Fig. 1(c)–(e), meaning that it is difficult for Mn to enter into the lattice of Mg_2Ni phase, which is also reported in Ref. [22]. This phenomenon is probably explained as follows. Electronegativities of metal elements gradually increase along the sequence Mg < Mn < Ni. Therefore, due to the bigger difference of electronegativities between Ni and Mg in comparison with Mn, it is much easier for bonding between Mg and Ni. As a result, it is difficult for Mn to substitute the site of Ni in Mg_2Ni lattice. Fig. 2 shows X-ray diffraction patterns of the $Mg_2Ni_{0.25}Mn_{0.75}$ alloys with different milling times. After 4 h of milling, the intensities of the diffraction peaks of Mg, Ni and Mn decrease and their peak widths increase as a result of the reduction of crystallite size and/or the accumulation of microstrain during MA. When milling duration is 8 h, the peaks of Mg_2Ni phase appear, while the peaks of Mg and Ni nearly disappear. Although the milling time is prolonged to 24 h, there are still the Mn peaks of high intensity, which further proves the solid solubility of Mn in Mg_2Ni phase is low.

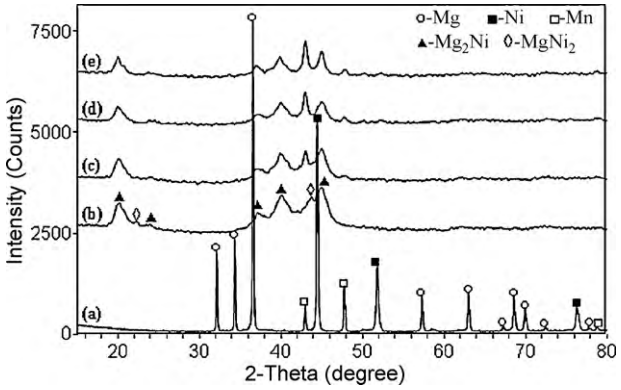

Fig. 1. X-ray diffraction patterns of the initial elemental powder mixture (a) and the $Mg_2Ni_{(1-x)}Mn_x$ alloys with a fixed milling time of 8 h: (b) x = 0, (c) x = 0.125, (d) x = 0.25 and (e) x = 0.375.

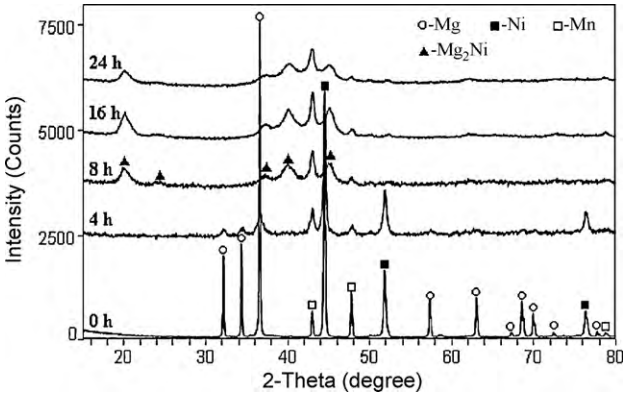

Fig. 2. X-ray diffraction patterns of the initial elemental powder mixture (0 h) and the $Mg_2Ni_{0.25}Mn_{0.75}$ alloys with different milling times.

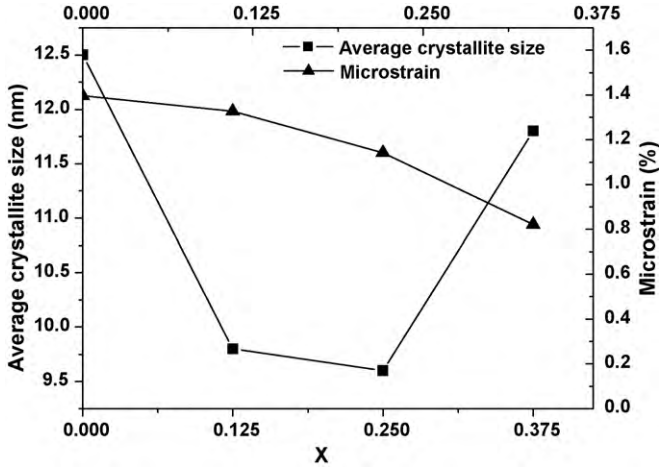

Fig. 3. Evolution of average crystallite size and microstrain of $Mg_2Ni_{(1-x)}Mn_x$ ($x = 0$, 0.125, 0.25, 0.375) alloys milled for 8 h versus x.

X-ray diffraction peak broadening shown in Fig. 1 is evaluated and the evolution of average crystallite size and microstrain for different substitution amounts of Mn for Ni is presented in Fig. 3. It is observed that within a fixed milling time (8 h), with the increase of substitution amount of Mn for Ni from $x = 0$ to $x = 0.375$, the average crystallite size decreases first from 12.5 nm to 9.6 nm and then increases from 9.6 nm to 11.8 nm with the minimum 9.6 nm obtained at $x = 0.25$, while the microstrain monotonously decreases from 1.39% to 0.82%. This result may be explained as follows. Both Mg and Ni are malleable and ductile, while Mn is hard and brittle. With the increase of substitution amount of Mn for Ni, the hardness and brittleness of MA powders substantially increase, which is favorable for the MA powders to get work hardened and causes more intensive collisions among powders, resulting in more easily fracturing of crystal grains. Therefore, the average crystallite size decreases first with the increase of Mn content from $x = 0$ to 0.25. With the concomitant decline of crystallite size, the grain boundary increases remarkably, which is beneficial to the defects to migrate out of the crystallites, and consequently promotes microstrain release. Additionally, due to the enhancement of brittleness of MA powders, the tendency to fracture predominates over deformation. Because of the fact that the deformation can introduce a great number of defects which can increase microstrain, the weakened tendency to deform leads to the decline of microstrain. As a result, the microstrain decreases with the increase of Mn content from $x = 0$ to 0.25. When the content of Mn increases to a certain extent ($x = 0.375$), the rise of temperature caused by more intensive collisions cannot be ignored and consequently accelerates the crystal grains growth and the lattice strain release, which is the probable reason why the crystallite size increases from 9.6 nm to 11.8 nm and the microstrain decreases from 1.14% to 0.82% for $Mg_2Ni_{0.625}Mn_{0.375}$ in comparison with that of $Mg_2Ni_{0.75}Mn_{0.25}$. Orimo and Fujii [1] reported that the average crystallite sizes of Mg_2Ni alloy reduced down to nearly 16 nm by milling for 3.6 ks according to the peak broadening of the X-ray diffraction profiles using Wilson method [23]. Due to using longer milling time (8 h) in this study compared with 3.6 ks, smaller average crystallite size (12.5 nm) is obtained for Mg_2Ni. MA is proved to strongly promote the formation of Mg_2Ni. In fact, traces of Mg_2Ni has already appeared after only 4 h of milling for $x = 0$ (Table 1). After formation of Mg_2Ni, the tendency to fracture is reinforced because of the brittle behavior of ordered intermetallic structures [24]. This is also supported by the phenomenon that the collisions noise began to rise after 3 h of milling, which reveals that the sample powder has become much harder. As a result, repeated strong ball-powder collisions significantly introduce the microstrain and cause the reduction of crystallite size. The induced microstrain can assist diffusion by reducing the hysteresis of hydrogen absorption and desorption [25]. The formation of nanocrystalline Mg_2Ni gives an

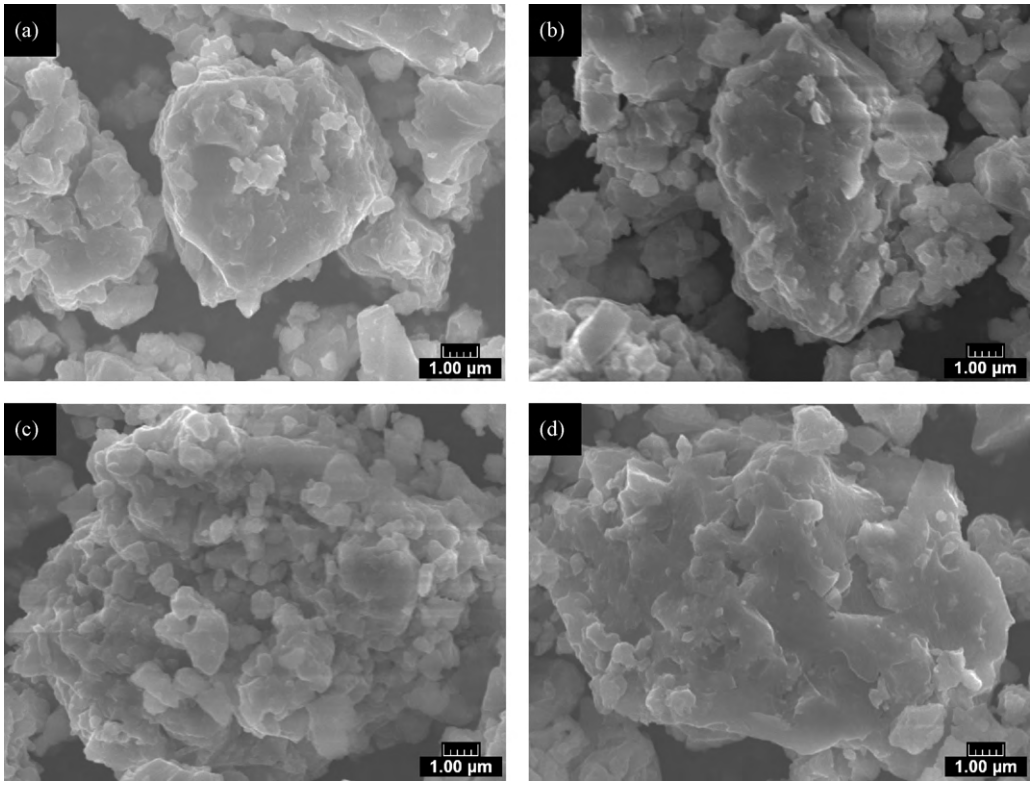

Fig. 4. SEM morphologies of the $Mg_2Ni_{(1-x)}Mn_x$ alloys with a fixed milling time of 8 h: (a) $x = 0$, (b) $x = 0.125$, (c) $x = 0.25$ and (d) $x = 0.375$.

enormously increased amount of grain boundaries which can provide easier channel for the diffusion of hydrogen atoms. At the same time, nanoscale Mg_2Ni alloy can avoid the long-range diffusion of hydrogen atoms through the already formed hydride phase [16]. So the hydriding/dehydriding kinetics can be improved due to the introduction of microstrain and reduction of crystallite size.

Fig. 4 shows the SEM morphologies of the $Mg_2Ni_{(1-x)}Mn_x$ ($x = 0$, 0.125, 0.25, 0.375) alloys with a fixed milling time of 8 h. It is observed that the powder particles in all the compositions are mainly flaky and show cleavage fracture morphology and inhomogeneous size distribution, which is the same as that observed by Gasiorowski et al. [12]. The powder particles are also agglomerates of many smaller particles (namely subparticles), which is because a large amount of energy of balling is transferred to particles, resulting in high concentration of defects and decrease of particle size, which increases the surface free energy of particles. In order to decrease the total energy of particles, subparticles agglomerate together to reduce the surface area for lowering surface free energy. The size of agglomerates shows the tendency of increase with the increase of x from 0 (Fig. 4(a)) to 0.375(Fig. 4(d)) excluding $x = 0.25$. It is noteworthy that the subparticles that constitute powder particles in Fig. 4(c) are much smaller than those in Fig. 4(a), (b) and (d). This is because with the increase of Mn content, the hardness and brittleness of MA powders increase, which is favorable for the particles to fracture. As a result, the subparticle sizes decrease when x increases from 0 to 0.25. Whereas, as mentioned above, excessive Mn ($x = 0.375$) enhances the collisions among particles, resulting in the substantial rise of temperature, which promotes the welding that tends to increase the particle size. As a result, the subparticle sizes rebound when x increases from 0.25 to 0.375. Therefore, there exist an optimal value of Mn content for obtaining smallest subparticles, namely $x = 0.25$. The smaller size of subparticles in Fig. 4(c) will significantly increase the surface area of the powder particles compared with the bigger ones in Fig. 4(a), (b) and (d), which will facilitate the absorption of hydrogen at the surface of Mg_2Ni alloy and improve the hydrogen storage properties of Mg_2Ni intermetallic compound. Yang et al. [17] measured the specific surface areas of $Mg_2Ni_{0.75}Mn_{0.25}$ and Mg_2Ni alloys and got the value of 3.9 m^2/g for $Mg_2Ni_{0.75}Mn_{0.25}$ and 3.8 m^2/g for Mg_2Ni, which indicates that substitution of Mn for Ni at $x = 0.25$ is indeed helpful for increasing the specific surface areas of the alloys.

4. Conclusions

Based on this study, the following conclusions can be obtained: (1) substitution of Mn for Ni could inhibit the formation of $MgNi_2$ phase that does not interact with hydrogen; (2) the solid solubility of Mn in Mg_2Ni phase is low; (3) with the increase of substitution amount of Mn for Ni from $x = 0$ to $x = 0.375$, the average crystallite size decreases first from 12.5 nm to 9.6 nm and then increases from 9.6 nm to 11.8 nm with the minimum 9.6 nm obtained at $x = 0.25$, while the microstrain monotonously decreases from 1.39% to 0.82%; (4) SEM morphologies indicate that the powder particles in all the compositions are mainly flaky and show cleavage fracture morphology and inhomogeneous size distribution. The sizes of subparticles of the composition $Mg_2Ni_{0.75}Mn_{0.25}$ are smaller than those of the other compositions, which indicates that the substitution of Mn for Ni at $x = 0.25$ is favorable for the increase of the surface areas of the Mg_2Ni intermetallic compound.

Acknowledgment

The authors would like to thank Mr. O. Rapaud for his technical assistance concerning SEM.

References

[1] S. Orimo, H. Fujii, Appl. Phys. A 72 (2001) 167–186.
[2] A. Züttel, Mater. Today 6 (2003) 24–33.
[3] M. Latroche, J. Phys. Chem. Solids 65 (2004) 517–522.
[4] L. Zaluski, A. Zaluska, J.O. Ström-Olsen, J. Alloys Compd. 217 (1995) 245–249.
[5] C.H. Chiang, Z.H. Chin, T.P. Perng, J. Alloys Compd. 307 (2000) 259–265.
[6] M. Jurczyk, W. Rajewski, G. Wójcik, W. Majchrzycki, J. Alloys Compd. 285 (1999) 250–254.
[7] G. Liang, J. Huot, R. Schulz, J. Alloys Compd. 320 (2001) 133–139.
[8] L. Schlapbach, A. Züttel, Nature 414 (2001) 353–358.
[9] L. Zaluski, A. Zaluska, P. Tessier, J.O. Ström-Olsen, R. Schulz, J. Alloys Compd. 217 (1995) 295–300.
[10] J. Huot, S. Bouaricha, S. Boily, J.-P. Dodelet, D. Guay, R. Schulz, J. Alloys Compd. 266 (1998) 307–310.
[11] Y.H. Zhang, X.Y. Han, B.W. Li, H.P. Ren, X.P. Dong, X.L. Wang, J. Alloys Compd. 450 (2008) 208–214.
[12] A. Gasiorowski, W. Iwasieczko, D. Skoryna, H. Drulis, M. Jurczyk, J. Alloys Compd. 364 (2004) 283–288.
[13] H.T. Yuan, L.B. Wang, R. Cao, Y.J. Wang, Y.S. Zhanga, D.Y. Yan, W.H. Zhang, W.L. Gong, J. Alloys Compd. 309 (2000) 208–211.
[14] L. Hima Kumar, B. Viswanathan, S. Srinivasa Murthy, J. Alloys Compd. 461 (2008) 72–76.
[15] C. Suryanarayana, Prog. Mater. Sci. 46 (2001) 1–184.
[16] L. Zaluski, A. Zaluska, J.O. Ström-Olsen, J. Alloys Compd. 253–254 (1997) 70–79.
[17] H.B. Yang, H.T. Yuan, J.T. Ji, H. Sun, Z.X. Zhou, T.S. Zhang, J. Alloys Compd. 330–332 (2002) 640–644.
[18] T. Kohno, M. Kanda, J. Electrochem. Soc. 144 (1997) 2384–2388.
[19] Y. Tsushio, E. Akiba, J. Alloys Compd. 267 (1998) 246–251.
[20] G.K. Williamson, W.H. Hall, Acta Metall. 1 (1953) 22–31.
[21] M. Terzieva, M. Khrussanova, P. Peshev, J. Alloys Compd. 267 (1998) 235–239.
[22] J. Woo, K. Lee, J. Electrochem. Soc. 146 (1999) 819–823.
[23] H.P. Klug, L.E. Alexander, X-ray Diffraction Procedures—For Polycrystalline and Amorphous Materials, 2nd edn, Wiley-Interscience, New York, 1974, p. 618.
[24] A. Ebrahimi-Purkani, S.F. Kashani-Bozorg, J. Alloys Compd. 456 (2008) 211–215.
[25] G. Liang, E. Wang, S. Fang, J. Alloys Compd. 223 (1995) 111–114.